RSC Advances

Volume 1 | Number 1 | Jan 2013 | Pages 1–100
RSC Advances
www.rsc.org/advances
ROYAL SOCIETY OF CHEMISTRY

This is an *Accepted Manuscript*, which has been through the Royal Society of Chemistry peer review process and has been accepted for publication.

Accepted Manuscripts are published online shortly after acceptance, before technical editing, formatting and proof reading. Using this free service, authors can make their results available to the community, in citable form, before we publish the edited article. This *Accepted Manuscript* will be replaced by the edited, formatted and paginated article as soon as this is available.

You can find more information about *Accepted Manuscripts* in the Information for Authors.

Please note that technical editing may introduce minor changes to the text and/or graphics, which may alter content. The journal's standard Terms & Conditions and the Ethical guidelines still apply. In no event shall the Royal Society of Chemistry be held responsible for any errors or omissions in this *Accepted Manuscript* or any consequences arising from the use of any information it contains.

ROYAL SOCIETY OF CHEMISTRY

www.rsc.org/advances

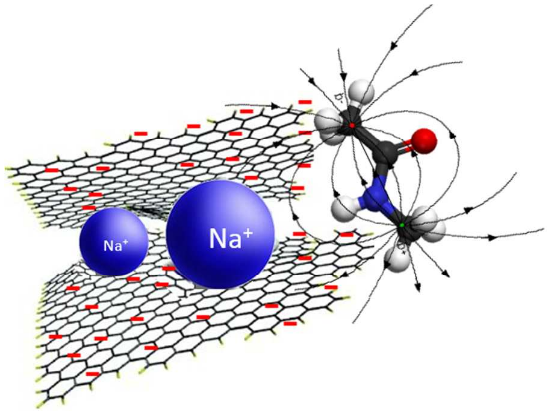
Na$^+$
Na$^+$

Advances RSCPublishing

Paper

Deep eutectic solvent based on sodium cation as an electrolyte for Supercapacitor application.

Cite this: DOI: 10.1039/x0xx00000x

W. Zaidi, L. Timperman, and M. Anouti *

Received 00th January 2012,
Accepted 00th January 2012

DOI: 10.1039/x0xx00000x

www.rsc.org/

Abstract

This study proposes a new deep eutectic solvent based on sodium nitrate and N-methylacetamide as an electrolyte for carbon-based supercapacitors at 80 °C. The reversible intercalation of ions into the graphitized ultra-micropores of activated carbon, separately detected at negative and positive electrodes, permits high pseudo-capacitance (up to 302 $F.g^{-1}$). The SEM/EDX mapping and XRD profile shows homogeneous distribution of Na in negative polarized electrodes indicating that sodium is well incorporated in the ultra-micropores of the carbon structure. The good capacitance obtained at 80°C in two-electrode cells at an operating voltage up to 2.0 V remained stable after 1000 charge-discharge cycles. Based on its physicochemical properties, as well as its electrochemical performances and stabilities, the sodium based DES can be considered a promising electrolyte for supercapacitor applications.

1. Introduction

Supercapacitors (SCs) attract increasing attention because of their high power density, long life cycle, short charging time and the fact that they are more economical and environmentally friendly than traditional batteries[1]. The most important challenge for SCs today is to increase their energy density to bring them closer to that of batteries. This can be achieved by increasing capacitance C, which is controlled by the carbon/electrolyte interface. Several studies have recently focused on the intercalation process in carbons affected by the nature of the carbon material, applied voltage/potential, intrinsic ions and solvent properties[2]. Currently, there is broad debate on the nature of the sites accessible to desolvated-ion intercalation: are they the ultra micropores, or the spaces between the dispersed graphitic layers. Gogotsi *et al.*[3] addressed the specific effect of pore size and pore-size distribution on the performance, by analyzing various carbons in diverse electrolytes. Their results stressed the effects of ion desolvation enabling access to the small pores that can be reached with "optimal" pore size, which depends on the ion size and the operating voltage.

Both aqueous and non-aqueous organic solutions can be used as electrolytes for supercapacitors. Currently, aqueous (e.g., H_2SO_4, KOH, Na_2SO_4) and organic (e.g. Et_4NBF_4 in acetonitrile, $LiBF_4$ in propylene carbonate) solutions are widely utilized [4]. The main drawback of aqueous electrolyte-based supercapacitors is their narrow cell voltage (limited to 1.2 V) and hence low energy density[5]. Organic electrolytes have relatively larger electrochemical windows (>2.7 V), however their flammability, toxicity, and environmentally hazardous nature are the main problems of these electrolytes. Room temperature ionic liquids (RTILs) are also regarded as potentially safer electrolytes for supercapacitors thanks to their unique physical and chemical properties, which are considered interesting advantages[6-8]. Compared with conventional organic electrolytes, RTIL electrolytes can improve the safety and capacity retention of supercapacitors. On the other hand, the high viscosity of commonly used ionic liquids such as EMImBF4 (37.7 cP), $BMImBF_4$ (233 cP) and EMImTFSI (28 cP) limit the performance of the devices[9]. The relatively high viscosity of ionic liquids is due to the relatively large radii ions in comparison to the average radius of the voids. It has recently been shown that the viscosity of a fluid is related to the free volume and the probability of finding holes of suitable dimensions for the solvent molecules/ions to move into[10].

Deep eutectic solvents (DES) are a eutectic mixture of salt and hydrogen bond donor compounds (HBD) in a specific ratio forming eutectics by the depression of the freezing point[11]. DESs are easier to synthesize by mixing cheaper raw materials with good biocompatibility, they have higher stability windows and good conductivities[12]. DESs share many characteristics with conventional ILs (e.g. non-reactive with water, non-volatile and biodegradable, among others), but their low cost make them particularly attractive (more than ILs) in many applications such as those requiring large scale synthesis, including those designated as electrolytes for energy devices. Furthermore, DESs can be customized to suit large-scale applications thanks to their unexpected solvent properties which enable them to dissolve metal oxides.[13] Unfortunately, the potential application of DESs as electrolytes has not been investigated in sufficient detail. In recent studies we have demonstrated that the

EDLC capacity in DESs based on lithium salt and N-methylacetamide (MAc) can be described by both pure double layer adsorption and by the insertion of “free” ions into the ultra-micropores of the activated carbon material[14]. To replace the lithium based energy storage technology, the sodium systems are considered as very promising solutions owing to the high abundance and low cost of sodium resources as well as the low Na^+/Na redox potential[15]. Unfortunately, only limited numbers of electrolytes based on sodium ions are available so far. Although the organic solutions, usually carbonates of a Na salt such as $NaClO_4$ and $NaPF_6$ are widely used in Na secondary batteries[16-18]. In this study, we report for the first time on low cost and easy formulated sodium based non-aqueous electrolytes for supercapacitors. Unlike conventional salts in aqueous or organic media, $NaNO_3$/ MAc deep eutectic solvents permit easy insertion of desolvated sodium cations into activated carbon (AC).

2. Experimental

Anhydrous sodium nitrate ($NaNO_3$) (99.8%) and N-methylacetamide (MAc) (97%) were purchased from Sigma Aldrich. A $NaNO_3$/ MAc deep eutectic solvent was formulated by mixing $NaNO_3$ (0.1 mol) and distilled MAc (0.9 mol) at room temperature. The transparent low-viscous liquid $NaNO_3$/MAc DES presents conductivity, σ = 3.17 mS.cm^{-1}, and viscosity η = 12.63 mPa.s at 25 °C. DES was conserved in a glove box before use. The water content analyzed by Karl-Fisher titration was 200 ppm.

Electrochemical measurements were carried out on a Versatile Multichannel Potentiostat (Biologic S.A) by cyclic voltammetry or galvanostatic charge-discharge using a Teflon Swagelok®-type system with three-electrodes (or two-electrodes). Activated carbon was used as the working and counter electrodes and an Ag wire as the pseudo-reference electrode. The separator was Whatman® glass microfiber paper. The AC electrode with polyvinylidene fluoride (PVDF) binder (AC/PVDF/carbon black; 80/10/10 weight %) was kindly supplied by “Bleu Solution”. The AC exhibits a specific surface area of 1500 m^2 g^{-1} (BET), with high microporosity (d < 1 nm). For all electrochemical characterization the temperature was controlled at 80°C by a thermostatic oven. The electrode material was observed after cycling by scanning electron microscopy (SEM-FEI quanta 200) combined with energy dispersive spectroscopy (EDS-Inca X act Oxford instruments). X-ray diffraction analysis was carried out with an X-ray diffractometer (model D8 Bruker) using a Cu Kα radiation (λ= 0.15409 nm).

3. Results and discussion

3.1 Physicochemical characterization of $NaNO_3$/Mac electrolyte

The formulating of the DES as electrolytes (composition) is conducted by the optimization of transport properties, in the case of mixtures with sodium nitrate; the viscosity increases with the addition of salt even if the mixture remains liquid. The best compromise between fluidity and a liquid state at 25°C is obtained for $NaNO_3$/Mac (x_{Na} = 0.1). This composition is chosen for this study. Vapor pressure of $NaNO_3$/MAc DES was measured by the VLE method as previously described by our group[19, 20]. In this method, the vapor pressure of the liquid solution was measured during the equilibration process at a given temperature, T_{eq} before degassing the solution by successive melting/freezing cycles. The experimental vapor pressures for $NaNO_3$/Mac (x_{Na} = 0.1) DES at T_{eq} = 20°C, 60°C and 80°C was respectively 2.24 mbar, 6.33 mbar and 10 mbar. These values are lesser than conventional organic electrolytes for EDLC such as acetonitrile (97 mbar at 20°C), ref or aqueous sulfuric acid solution (5, 56 mbar) at 20°C [21].

Figure 2 presents the evolution of the conductivity and viscosity as a function of the temperature. As can be seen, the conductivity (η) for $NaNO_3$/Mac (x_{Na} = 0.1) DES measured in this work ranges from 1.86 mS.cm^{-1} at 10°C and reaches 21.15 mS.cm^{-1} at 75°C. The conductivity of lithium homologue $LiNO_3$/Mac (x_{Li} = 0.25) was measured as 0.76 mS cm^{-1} at 25°C and 6.5 mS.cm^{-1} at 80°C.

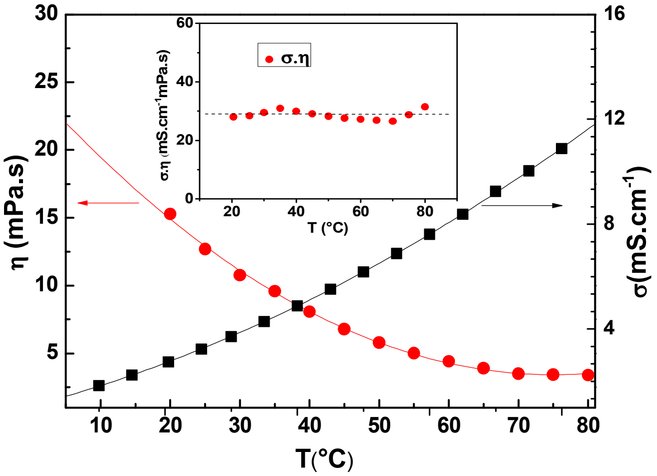

Figure 1. Evolution of the conductivity, s, viscosity, h, and Walden product (W = $\sigma.\eta$) as a function of the temperature for the mole fraction of sodium in the DES mixture x_{MAc} = 0.9).

As for most common electrolytes, the Walden’s product ($\sigma.\eta$) of $NaNO_3$/MAc DES, representing the compensation for increasing in mobility by increasing fluidity (η^{-1}) as a function of temperature is approximately constant with temperature (see inset in figure 1). Consequently, as the ions move through the solvent, the two forces driving the ions: mobility in the electric field and the frictional force of viscous flow, act in opposite directions, and the ions quickly reach a terminal speed. The calculated Walden product for $NaNO_3$/Mac (x_{Na} = 0.1) is (28.4 ± 1 mS.cm^{-1}.mPa.s) in a temperature interval (25 to 80) °C. By comparison $LiNO_3$/Mac (x_{Na} = 0.25) is over two times higher with (81.32 ± 1 mS.cm^{-1}.mPa.s) at the same temperature ranges.

3.2. Electrochemical study.

Figure 2 shows cyclic voltammograms recorded at v = 5 mV.s^{-1} with $NaNO_3$/Mac (x_{Na} = 0.1) such as the electrolyte in a three-electrode cell configuration using activated carbon as the working and counter electrode and Ag wire as the pseudo-reference.

Figure 1a visualizes the three first cycles for the negative electrode using [0.0V to - 0.8 V] versus Ag wire. The apparently easy Na^+ intercalation behavior into AC in the negatively potential range is shown by the cathodic peak at -0.5V vs Ag. The reversible cation intercalation is maintained during the successive cycles but the potential of this intercalation varies greatly and randomly according to the cycle number (Figure 2a). We can clearly show that all voltammograms present evident intercalation-de-intercalation behavior in addition to the adsorption part, which can be estimated from the dashed rectangle in figure 1a. For cycle 3, the shape of the voltammograms is more rectangular (CV blue and purple) indicating that the insertion of the Na^+ cation is easier in previously formed micro-cavities.

For the positively polarized electrode, figure 1b shows the seven successive first cycles using [0.0V to + 0.5 V] as potential versus Ag wire. The upward curve corresponds to the charge process, nitrate anion adsorption and intercalation, whereas the downward curve corresponds to the reversible discharge process. Here the peak attributed to the nitrate ions intercalation is more obvious.

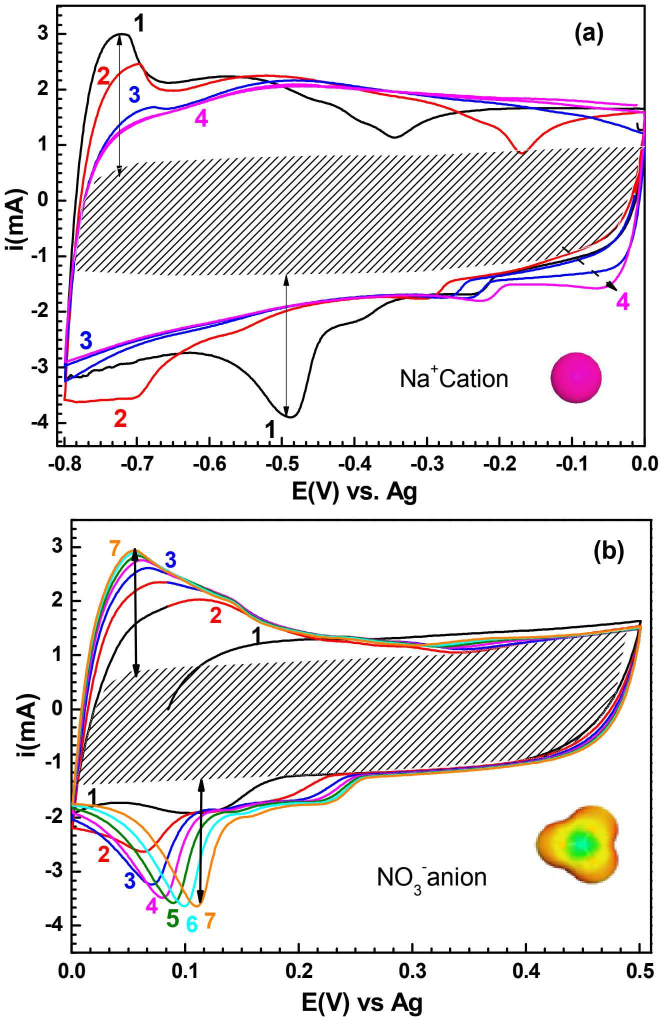

Figure 2. Cyclic voltammograms of activated carbon in NaNO$_3$/Mac (x_{Na} = 0.1). (a), negative electrode; (b), positive electrode, v = 5 mV s^{-1}, at 80°C. In the inset, the schematic COSMO volume, *V*, in cubic Angstroms of ions

During the first four cycles, the intensity of the couple of peaks at + 0.07 and + 0.1 V increases. For the following three cycles the intercalation de-intercalation mechanism becomes more electrochemically irreversible, as demonstrated by the spacing between the upward and downward peaks. Furthermore, the large peak in the negative electrode excluding the ionic adsorption illustrated by the rectangular dashed shape was higher than that of the positive electrode, indicating the superior intercalation capability of cations over anions, resulting in a higher capacitance in the negative electrode. This clearly indicates that it is easier to perform the intercalation of small ions, especially those with a low polarizability such as sodium cations. Certainly, desolvated Na$^+$ ions being weakly polarizable, they need a lower electric field in order to squeeze between the graphene layers. The very weak interaction of ions in MAc as a solvent leads to easily desolvated ions. Several authors, such as P. Simon *et al* and Y. Gogotsi *et al*. have suggested that the partial or total desolvation of ions is possible so that the ions can penetrate into the very small pores of the carbon electrodes[3]. Therefore, desolvation becomes easier in MAc-based DES electrolytes, consequently for these electrolytes a lower electric driving force for intercalation is required.

Activated carbons (ACs) are amorphous porous materials[4]. They are composed of small graphitic crystallites, whose random stack is responsible for their porosity[22]. Models which are intended to represent the structure of inter-crystallite pores consist of curved and twisted graphene sheets enclosing randomly shaped pores[22]. Graphene sheets are known to be highly flexible, It is believed that the space between small graphene layers in carbons is inaccessible to ions because they are closely folded together in order to reduce surface energy[23]. However, induced polarization by electrostatic forces or a high dielectric solvent can lead to the intercalation of ions and solvent molecules into the interlayer space, leading to supercapacitors with a high specific capacitance[24].

Due to its “water-like” physical properties (e.g. very high dielectric constant (ε = 178.9), high dipolar moment μ = 6.8 D), N-methylacetamide as a solvent presents the ideal conditions for reducing surface energy in graphene sheets leading to the intercalation of ions. The strong interaction of the acetamide (-CO-NH-CH$_3$) groups with ions (cations and anions) can lead to the formation of coordinated complexes producing micro-domains in solution as demonstrated by infrared and dielectric relaxation measurements[25]. The (N–H–O) hydrogen bond in the solvent explains the solid state of MAc at room temperature, by adding NaNO$_3$ the interaction between MAc and salt weakens or even breaks this intra (N–H–O) hydrogen bond due to the competitive Na$^+$–O interactions in solution. With these new room temperature molten salt electrolytes, besides considering the applied voltage window in electrochemical systems like supercapacitors, the ion dimensions and solvent polarizability should also be considered. Certainly, the high dielectric constant of MAc can improve ion intercalation by enhancing the surface energy of graphene sheets due to local high polarization of MAc.

In order to simultaneously monitor the intercalation behavior of NO$_3^-$ and Na$^+$ in both positive and negative polarization, we polarized the working electrode from the open-circuit potential using the standard three-electrode cell from -1.2 V to 0.8 V vs. Ag wire (figure 2). Several peaks were observed, their potential and intensity varies randomly with each cycle. For example, in cycle 11, four peaks are observed at 0.5 V, -0.4 V, -0.7 V and -1.1 V respectively, in the forward scan in which only one area of positive polarization is observed.

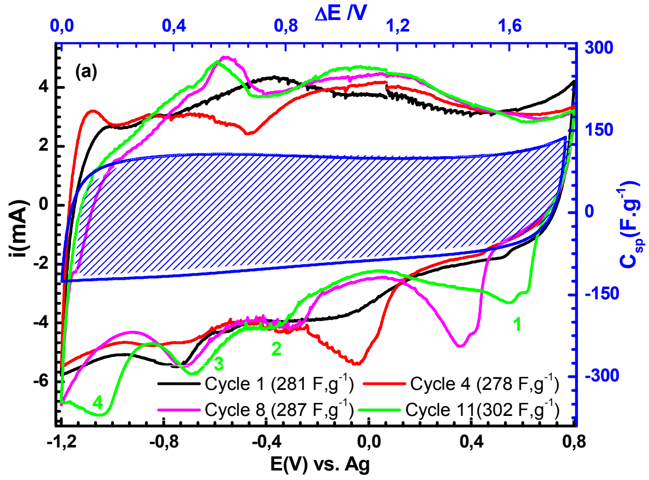

Figure 3. Cyclic voltammograms for three-electrode cells, and two-electrode cells (blue dashed curve) for activated carbon in in NaNO$_3$/Mac (x_{Na} = 0.1) at v = 5 mV s^{-1}, at 80°C.

Generally in highly ordered structures such as graphitic structures, spinels, or lamellar materials, (such as “birnessite-type” MnO_2 etc. ion intercalation is observed at constant potential. Here, activated carbon as we explained in the introduction, is composed by small graphitic crystallites, whose random stack is responsible for their porosity. By consequence these typical structures provide the disordered intercalated ions seat when the potential increases to random potentials. When the polarized system between two electrodes, one of the two electrodes is limiting, it prevents the insertion of ions in the second electrode, the potentials of the electrodes is interdependent. However when polarizes the working electrode against a reference electrode, the two electrodes are working alternatively in independent potential.

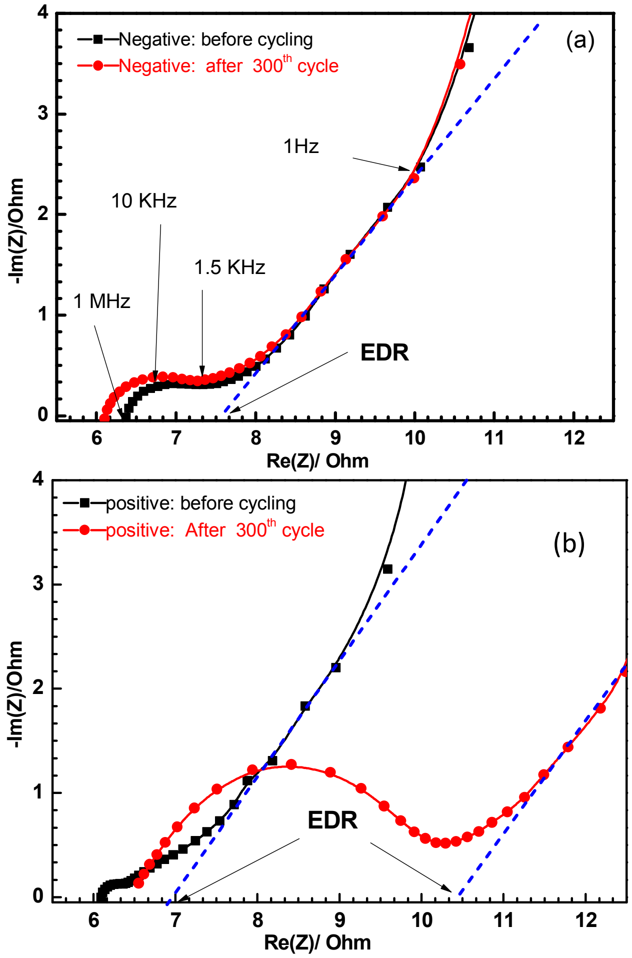

Figure 4. Electrochemical impedance spectroscopy plots of negative (a) and positive (b) AC electrodes in the three electrode cells recorded at 80 °C in $NaNO_3$/Mac (x_{Na}= 0.1) at v = 5 mV s^{-1}, at 80°C.

The specific gravimetric capacitance (C_{sp}) was calculated using

$$C_{sp} = \frac{2\int idt}{\Delta E.m} \qquad \text{eq 1}$$

where ΔE is the operating voltage, *i* is the discharge current, and *m* is the mass of active material (carbon) of the working electrode in each cycle; these are 281, 278, 287 and 302 Fg^{-1} for cycles 1, 4, 8 and 11 respectively. Pure adsorption as indicated by the blue shaded rectangle was obtained by cycling in a two-electrode system with an operating voltage of ΔE = 1.8 V, wherein no insertion is observed under these polarizing conditions. This observation can be explained by the successive polarization of the working electrode, which allows the full opening of small “stacks” of graphitic layers or very small pores, thus creating new sites accessible to the ions. We assume that ions are totally desolvated and then squeezed into the narrow graphitic layers. The activated carbon material is then able to provide a higher specific capacitance from 281 $F.g^{-1}$ in the first cycle up to 302 $F.g^{-1}$ at cycle eleven, even at a lower applied voltage window (ΔE = 2V).

Figure 4 compares the Nyquist plots before and after cycling for negative (figure 4 a) and positive (figure 4b) AC electrode in three-electrode cells recorded at 80 °C. The low-frequency region corresponds to purely capacitive phenomena and is represented by a quasi-vertical line (figure4). The associated resistance, called equivalent diffusion resistance (EDR), is obtained from the intercept of the line with the Z′-axis. The relatively small and similar Warburg region initially obtained for both electrodes indicates low ion diffusion impedance, actually driving a lower obstruction of the ion movement. In the case of a positive electrode (figure 4b), a significant enhancement in the resistance of ionic resistance in the carbon porosity is displayed after cycling by an increase of EDR values, which indicates the irreversible insertion of anions into the micro porosity of the activated carbon electrode.

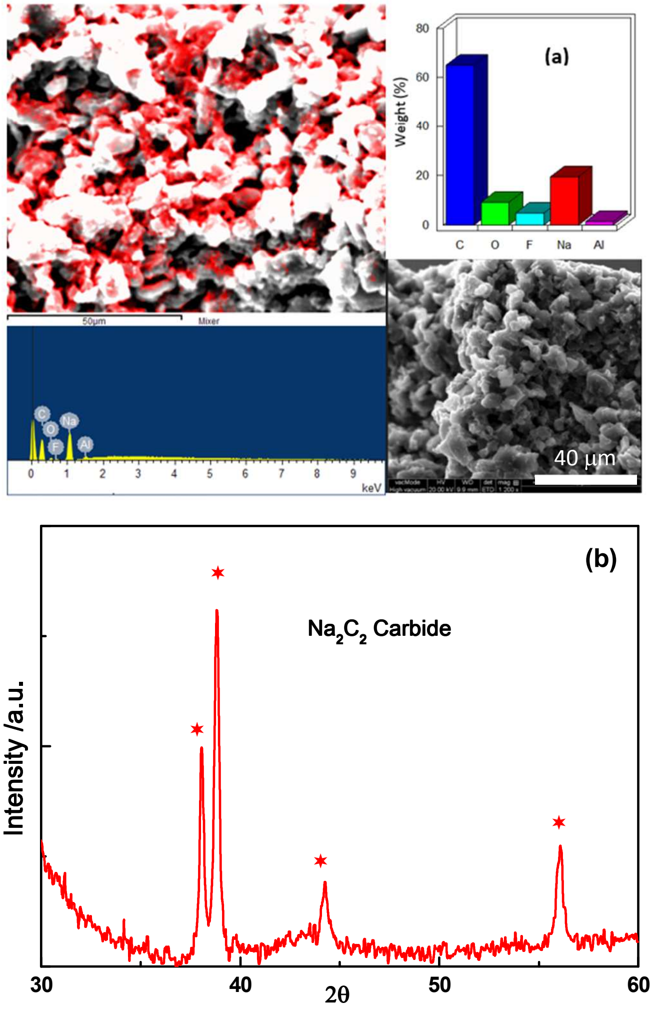

Figure 5. SEM, EDX mapping (a) and XRD profile (b) for activated carbon electrode after 11th cycle. Red color represents the sodium element.

After polarization by cycling, the negative electrode was analyzed by EDS and XRD profile as shown in figure 5a. The SEM/EDS analyses show homogeneous distribution of Na (20 % weight) in electrodes indicating that sodium is well incorporated in the carbon structure. The assimilated to the Na_2C_2 carbide phase is detected by XRD profile[26] figure 5b.

The test cycling performances of Na-DES at AC electrode, were also performed by the galvanostatic method in symmetric two-electrode cells at a current density of 200 $mA.g^{-1}$, $\Delta E = 1.8$ V and T = 80°C as shown in figure 6. The discharge cycle (inset in figure 6) was used to determine the specific capacitance (C_{sc}), which was calculated using (eq 2)

$$C_{sp} = \frac{2.i}{m.\left[\frac{dV}{dt}\right]} \qquad \text{eq 2}$$

where *m* is the mass of one electrode and *dV/dt* is the slope of the discharge curve. Stability tests indicated that the capacitance evolved from 100 to 80 $F.g^{-1}$ after 1000 cycles (inset in figure 6), so confirming that no insertion of ions was observed at this applied tension or that irreversible insertion limits the capacitance.

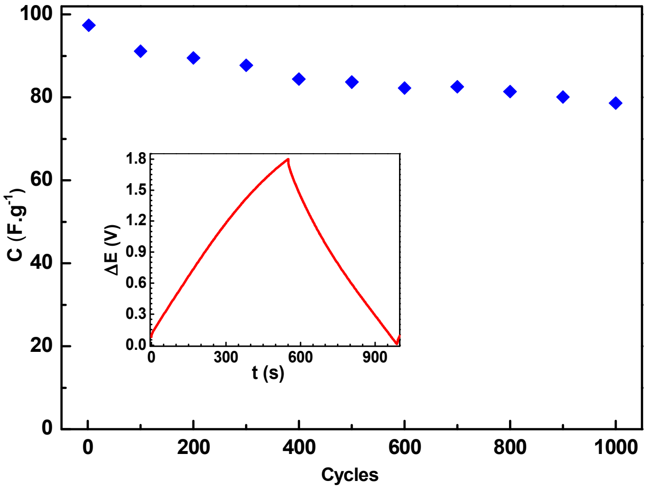

Figure 6. Galvanostatic charge-discharge curves (inset) and capacitances calculated from eq (2) at a current density of 200 mA g^{-1} for 1000 cycle for activated carbon electrode with $LiNO_3$-MAc ($x_{Na^+} = 0.25$) as electrolyte at 80 °C.

Conclusions

The DES electrolyte based on N-methylacetamide and sodium nitrate was tested as an electrolyte for an activated carbon based supercapacitor at 80°C. The electrochemical behavior in negative or positive polarization demonstrates the simultaneous intercalation behavior of NO_3^- and Na^+. The SEM/EDX mapping and XRD profile show homogeneous distribution of Na as Na_2C_2 phase in negative polarized electrodes indicating that sodium is well incorporated in the ultra-micropores of the carbon structure. It is clear that the goal now is to propose a solution to improve reversible intercalation of ions in the two electrodes system by adapting for example porous carbons size to non-solvated Na^+ ions, this study is currently being conducted in the laboratory. The Na-DESs electrolytes can be promising electrolytes, especially in sodium-based hybrid electrochemical systems.

Notes and references

PCM2E, EA 6299, Université F. Rabelais, Parc de Grandmont, 37200 Tours, France. * E-mail: meriem.anouti@univ-tours.fr. Fax: (33)247367360. Tel: (33)247366951.

1. K. Naoi, W. Naoi, S. Aoyagi, J.-i. Miyamoto and T. Kamino, *Accounts of Chemical Research*, 2012, **46**, 1075-1083.
2. E. Ventosa, W. Xia, S. Klink, F. La Mantia, M. Muhler and W. Schuhmann, *Electrochimica Acta*, 2012, **65**, 22-29.
3. M. Fukano, T. Fujimori, J. Ségalini, E. Iwama, P.-L. Taberna, T. Iiyama, T. Ohba, H. Kanoh, Y. Gogotsi, P. Simon and K. Kaneko, *The Journal of Physical Chemistry C*, 2013, **117**, 5752-5757.
4. F. Béguin, V. Presser, A. Balducci and E. Frackowiak, *Advanced Materials*, 2014, **26**, 2219-2251.
5. F. Béguin and E. Frackowiak, *Supercapacitors: Materials, Systems, and Applications*, Wiley-VCH, Germany, 2013.
6. A. Balducci, R. Dugas, P. L. Taberna, P. Simon, D. Plée, M. Mastragostino and S. Passerini, *Journal of Power Sources*, 2007, **165**, 922-927.
7. L. Conte, G. Gambaretto, G. Caporiccio, F. Alessandrini and S. Passerini, *Journal of Fluorine Chemistry*, 2004, **125**, 243-252.
8. M. Kunze, S. Jeong, G. B. Appetecchi, M. Schönhoff, M. Winter and S. Passerini, *Electrochimica Acta*, 2012, **82**, 69-74.
9. M. V. Fedorov and A. A. Kornyshev, *Chemical Reviews*, 2014, **114**, 2978-3036.
10. A. P. Abbott, *ChemPhysChem*, 2004, **5**, 1242-1246.
11. A. P. Abbott, D. Boothby, G. Capper, D. L. Davies and R. K. Rasheed, *Journal of the American Chemical Society*, 2004, **126**, 9142-9147.
12. L. Bahadori, M. H. Chakrabarti, F. S. Mjalli, I. M. AlNashef, N. S. A. Manan and M. A. Hashim, *Electrochimica Acta*, 2013, **113**, 205-211.
13. Q. Zhang, K. De Oliveira Vigier, S. Royer and F. Jerome, *Chemical Society Reviews*, 2012, **41**, 7108-7146.
14. W. Zaidi, A. Boisset, J. Jacquemin, L. Timperman and M. Anouti, *The Journal of Physical Chemistry C*, 2014.
15. K. Kuratani, M. Yao, H. Senoh, N. Takeichi, T. Sakai and T. Kiyobayashi, *Electrochimica Acta*, 2012, **76**, 320-325.
16. C. Ding, T. Nohira, R. Hagiwara, K. Matsumoto, Y. Okamoto, A. Fukunaga, S. Sakai, K. Nitta and S. Inazawa, *Journal of Power Sources*, 2014, **269**, 124-128.
17. J. Y. Jang, H. Kim, Y. Lee, K. T. Lee, K. Kang and N.-S. Choi, *Electrochemistry Communications*, 2014, **44**, 74-77.
18. D. Monti, E. Jónsson, M. R. Palacín and P. Johansson, *Journal of Power Sources*, 2014, **245**, 630-636.
19. Y. R. Dougassa, J. Jacquemin, L. El Ouatani, C. Tessier and M. Anouti, *The Journal of Physical Chemistry B*, 2014.
20. Y. R. Dougassa, J. Jacquemin, L. El Ouatani, C. Tessier and M. Anouti, *The Journal of Chemical Thermodynamics*, 2014, **79**, 49-60.
21. E. W. Hornung and W. F. Giauque, *Journal of the American Chemical Society*, 1955, **77**, 2744-2746.
22. J. F. H. Peter, L. Zheng and S. Kazu, *Journal of Physics: Condensed Matter*, 2008, **20**, 362201.
23. P. Simon and Y. Gogotsi, *Accounts of Chemical Research*, 2012, **46**, 1094-1103.

24. S. Kondrat, C. R. Perez, V. Presser, Y. Gogotsi and A. A. Kornyshev, *Energy & Environmental Science*, 2012, **5**, 6474-6479.
25. S. F. Abdulnur and K. Laki, *Biophysical Journal*, 1979, **28**, 503-509.
26. S. Hemmersbach, B. Zibrowius and U. Ruschewitz, *Zeitschrift für anorganische und allgemeine Chemie*, 1999, **625**, 1440-1446.